Adduct-based p-doping of Organic Semiconductors

Nobuya Sakai¹, Ross Warren¹, Fengyu Zhang², Simantini Nayak^{3,4}, Junliang Liu⁵, Sameer V. Kesava¹, Yen-Hung Lin¹, Himansu S. Biswal⁶, Xin Lin², Chris Grovenor⁵, Tadas Malinauskas⁷, Aniruddha Basu⁸, Thomas D. Anthopoulos⁸, Vytautas Getautis⁷ Antoine Kahn², Moritz Riede¹, Pabitra K. Nayak^{*1,9} and Henry J. Snaith^{*1}

- ¹ Clarendon Laboratory, Department of Physics, University of Oxford, Parks Road, Oxford OX1 3PU, UK
- ² Department of Electrical Engineering, Princeton University, Princeton, New Jersey 08544, United States
- ³ Department of Chemistry, University of Oxford, Inorganic Chemistry Laboratory, South Parks Road, Oxford OX1 3QR, UK
- ⁴ Materials Chemistry Department, CSIR-Institute of Mineral and Materials Technology, Bhubaneswar, 751013, India
- ⁵ Department of Materials, University of Oxford, Parks Road, Oxford OX1 3PH, UK
- ⁶ School of Chemical Sciences, National Institute of Science Education and Research, 752050 Bhubaneswar, India
- ⁷ Department of Organic Chemistry, Kaunas University of Technology, Radvilenu pl. 19, Kaunas LT-50254, Lithuania
- ⁸ King Abdullah University of Science and Technology (KAUST), KAUST Solar Center (KSC), Physical Sciences and Engineering Division (PSE), Material Science and Engineering Program (MSE), 23955–6900, Thuwal, Kingdom of Saudi Arabia
- ⁹ TIFR Centre for Interdisciplinary Sciences, Tata Institute of Fundamental Research, Hyderabad, 500046, India

Email: pabitra.nayak@tifrh.res.in; henry.snaith@physics.ox.ac.uk

Abstract

Electronic doping of organic semiconductors is essential for their usage in highly efficient optoelectronic devices. While molecular and metal complex-based dopants have enabled the much-needed progress of organic semiconductor-based devices, the bespoke organic emissive, charge transporting, and dopant materials remain a key cost driver for organic light emitting diodes (OLEDs). If a widespread transition towards larger area organic electronic devices is to occur, then there remains a need for clean, efficient and low-cost dopants. Here, we report dimethyl sulfoxide adducts as p-dopants fulfilling these conditions for a range of

organic semiconductors. These adduct based dopants are compatible with both solution and vapour phase processing. We explore the doping mechanism and use the knowledge we gain to "decouple" the dopants from the choice of counterion, which is not feasible with the existing class of p-dopants. We demonstrate that graded p-doping is possible using solution processing routes, and demonstrate its use in metal halide perovskite solar cells and OLEDs. This opens a new path for controlled doping of organic semiconductors.

Organic semiconductors are used in a wide range of cutting-edge technologies such as light emitting diodes (LEDs), field-effect transistors (FET) and photovoltaic (PV) devices due to their structural and functional tuneability¹⁻⁵. Organic semiconductors usually have low charge carrier mobilities and low intrinsic conductivity, as compared to their inorganic counterparts. This, therefore, often necessitates doping to increase the number of charge carriers, leading to both filling traps and improvement in charge conductivity for device applications⁶⁻⁹. A wide range of molecular dopants have been used for p-type and n-type doping of organic semiconductors^{10–14}. However, challenges such as poor doping efficiency^{15,16} and doping instability¹⁷ still exist. Complex chemical structures of dopants require expensive synthesis and purification steps. Partial charge transfer via the formation of ground state charge-transfer complexes can occur for dopant-host systems 18, meaning that substantial amounts of dopant are required for effective doping, which can have adverse effects on the morphology of the host¹⁹. Dopant molecules become the counterions during the doping process and remain in the host organic semiconductor ¹⁴. Because the dopants and counterions are coupled, it is difficult to optimize their role separately. A further challenge is to achieve graded doping in a device stack, or selective doping on one side of a charge conducting layer, especially using solution processing route²⁰, which is needed for better performance of devices. There is clearly the need for reliable and inexpensive dopants that circumvents the issues we have mentioned above associated with the present class of dopants.

Solutions of dimethyl sulfoxide (DMSO) with hydrobromic acid (HBr) have been used in the past for the oxidation of organic molecules during material synthesis, such as diphenylethane to benzyl, and acetophones to arylglyoxals^{21–23}. They have also been used to alter the oxidization state of Pd^{2+} to Pd^{4+} in the synthesis of the inorganic compound $Cs_2PdBr_6^{24}$. Here, we report that DMSO-HBr adducts can act as effective and clean p-dopants for a wide range of organic semiconductors. Our approach is an *in-situ* formation of the

dopant from commercially available low-cost chemicals, without any complex synthetic routes. The doping process is clean where the by-products and unreacted doping agents leave the thin-film. We further show that it is possible to select the counterion independently, unlike previously reported p-dopants. We also present a solution processible route to achieve graded doping in organic semiconductor films, and demonstrate applications of the adduct-based doping process in metal halide perovskite-based solar cells and OLEDs.

We start by testing the ability of our proposed agents to dope a variety of organic semiconductors, which are used as hole transporting material (HTM), in solution. In Fig. 1a and Table S1, we show the chemical structure and ionization potentials of the selected HTMs, respectively. Here, we introduce to the HTM solution, a mixture of DMSO and HBr in ~1:2 molar ratio, which we denote as the adduct forming agent. We provide procedural details in the experimental section of the SI. Fig. 1b shows the absorbance spectra and the photographs of the HTM solutions before and after the addition of the adduct forming agent. We observe absorption features corresponding to oxidized organic molecules after the addition of the adduct forming agent into all the HTM solutions. We chose 2,2',7,7'-Tetrakis[N,N-di(4methoxyphenyl)amino]-9,9'-spirobifluorene (Spiro-OMeTAD) as the testbed and use it to investigate the evolution of the charged species in the solution. After the addition of the adduct forming agent, we observe an absorption peak related to Spiro-OMeTAD⁺ at ~510 nm (Fig. 1b and Fig. S1a)^{25,26}. On further increasing the concentration of adduct forming agent in the solution, the absorption peak at ~690 nm corresponding to Spiro-OMeTAD⁺⁺ appears (Fig. S1a). We estimate the doping efficacy, defined by the molar ratio of oxidized Spiro-OMeTAD to added DMSO, to be ~17.5 % (see Fig. S1b). To explore the possibility of doping the HTM using vapour phase techniques, we expose Spiro-OMeTAD thin-films to vapours of DMSO and HBr (See SI for the methods and Fig. S2). As we show in Fig. S3, there is a continuous increase in the absorbance corresponding to the oxidized species in the Spiro-OMeTAD thin-film at 510nm and 690 nm with increasing vapour exposure time. This indicates that our doping strategy is compatible with both solution and vapour phase processing, and moreover, can be performed in the vapour phase under atmospheric conditions.

To confirm that the change in absorbance spectra corresponds to p-doping, we show the current-voltage (I-V) curves of thin-film electrode-gap in-plane devices with and without doping (Fig. S4) and we estimate the conductivity of the HTM films. We find a 2-3 order magnitude increase in the conductivity for all the HTMs with ionization energy (IE) \leq 5.2 eV after doping (Table S1). In Fig S5 we show conductivity measurements for the material

with the deepest highest occupied molecular orbital (HOMO) we found that we could dope, with an IE of ~ 5.5eV. We also evaluate the conductivity of the doped spiro-OMeTAD films using a 4-probe method²⁷, which reach a maximum conductivity of $\sim 2 \times 10^{-3}$ S cm⁻¹ (Fig 1 (c)) for both solution and vapor phase doping process. This is higher than what has been achieved for this HTM with other dopants²⁸⁻³¹, such as with tris(2-(1*H*-pyrazol-1-yl)-4-tertbutylpyridine)cobalt(III) tri[bis(trifluoromethane)sulfonimide] (Co(III)TFSI) complex (see Fig. S6). High conductivity enables the use of thicker transport layer with negligible voltage loss. To gain further insight into the doping effect, we perform ultraviolet photoelectron spectroscopy (UPS), X-ray photoelectron spectroscopy (XPS) and Kelvin probe-based (KP) contact potential difference measurements on the HTM thin-films. We show the UPS spectra of the undoped and doped films of Spiro-OMeTAD in Fig. 1e and work function values measured by KP in Fig. S7, respectively. As expected for p-type doping, we see an increase in the work function of the doped film and a shift of the Fermi levels closer to the HOMO level of the HTM. In Fig. S8, we show the XPS spectra of the doped films. We observe C-1s,O-1s and N-1s peaks shifting to lower binding energies with an increase in the concentration of the adduct forming agent, which provides further confirmation of p-doping³². In Figure S9 we report similar UPS and XPS shifts upon doping for another HTM, N,N,N', N'-Tetrakis(4methoxyphenyl)benzidine (MeO-TPD).

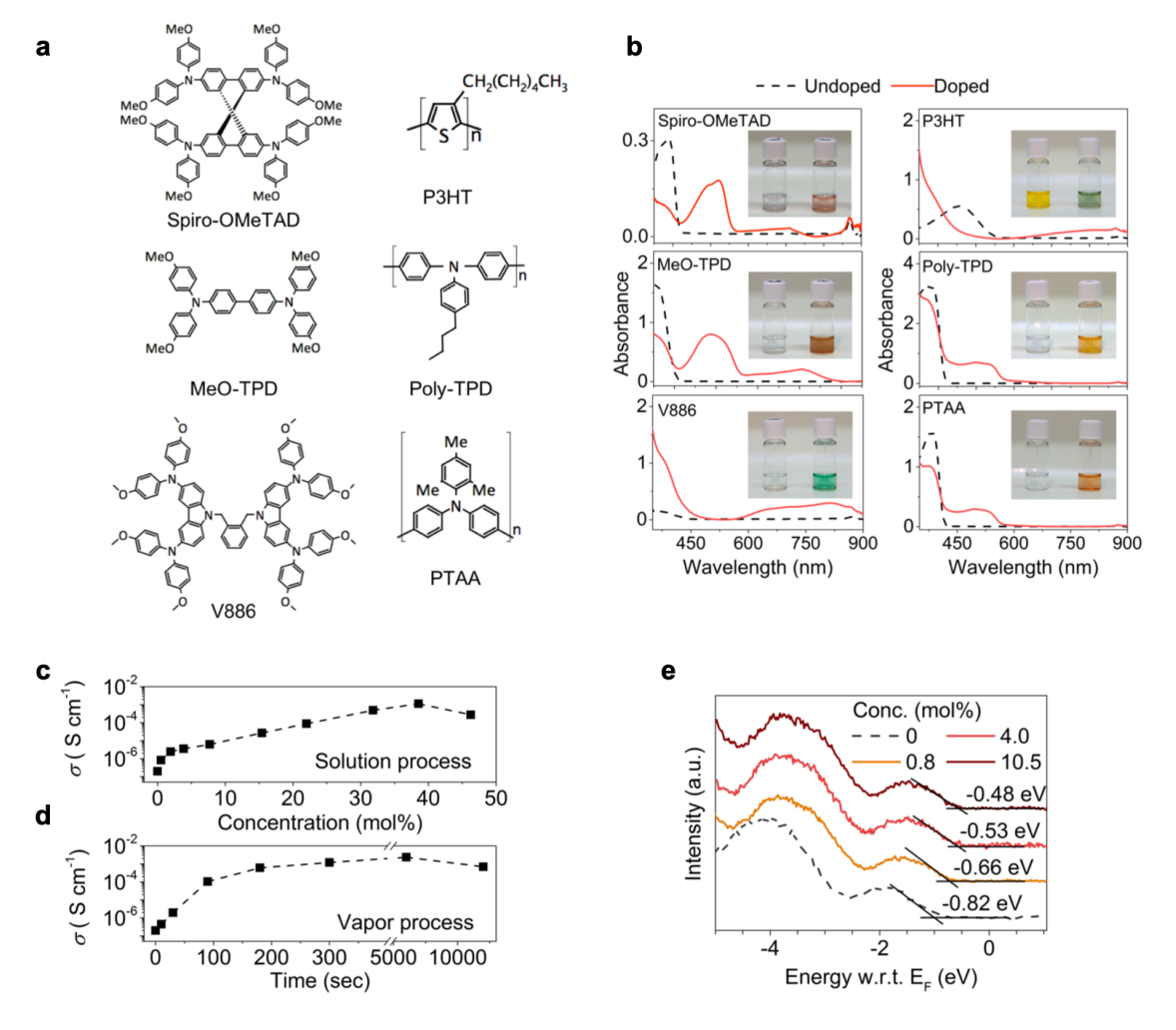


Figure 1| Doping ability of DMSO-HBr adduct for various hole-transporting materials. a, Chemical structures of hole-transporting materials (N2,N2,N2',N2',N7,N7,N7',N7'-octakis(4-methoxyphenyl)-9,9'-spirobi[9H-fluorene]-2,2',7,7'-tetramine (Spiro-OMeTAD), N,N,N',N'-tetrakis(4-methoxyphenyl)benzidine (MeO-TPD), 1,2-bis[3,6-(4,4'-dimethoxydiphenylamino)-9H-carbazol-9-methyl]benzene (V886), poly(3-hexylthiophene-2,5-diyl) (P3HT), poly[N,N'-bis(4-butylphenyl)-N,N'-bisphenylbenzidine] (Poly-TPD)) and poly[bis(4-phenyl)(2,4,6-trimethylphenyl)amine] (PTAA). b, UV-vis absorption spectra of organic HTMs in chlorobenzene (1-9×10⁻⁶ M) before (dotted line) and after (solid) the addition of the adduct forming agent. Insets: photographs of vials containing the neat HTM solution (left) and HTM solution with the adduct forming agent (right). c, d, Conductivity of the Spiro-OMeTAD thin-film doped with DMSO-HBr by either adding the dopant directly to the HTM solution (c: solution process) or exposing the thin films to DMSO-HBr vapor (d: vapor process). d, UPS spectra of the un-doped and doped (solution process) Spiro-OMeTAD thin-films.

The fact that neither DMSO nor HBr can dope the HTMs alone indicates that it is essential for both compounds to come together for the doping process to happen (see Fig. S10). Here, we investigate the doping mechanism by in-situ attenuated total reflection Fourier transform infrared spectroscopy (ATR-FTIR) and gas chromatographic mass spectrometry (GC-MS). In the FTIR spectrum of a DMSO solution in chlorobenzene, (Fig. 2a) we observe that the peak around ~1060 cm⁻¹, which corresponds to the absorbance of the S=O bond³³ of DMSO, broadens and shifts to lower wavenumber (around 1020-1050 cm⁻¹) after the addition of HBr, indicating the lowering of the S=O bond strength^{24,33}. Based on quantum chemical calculations, we assign the peaks around ~1035 - 1055 cm⁻¹ to the formation of a molecular adduct between DMSO and HBr (See Fig. S11). We then add the Spiro-OMeTAD solution to the adduct solution and record the change in the absorbance spectra over time. We observe a continuous decrease in the peak intensity at ~1050 cm⁻¹, indicating the consumption of the DMSO-HBr adduct and breaking of the sulfur-oxygen bond (see Fig. S12). Concurrently, we also record an increase in the absorbance of OH stretching around ~ 3400 cm⁻¹ (Fig. 2b)³⁴, indicating that H₂O is one of the by-products of the process. Via GC-MS of the released gases during the doping process, we identify dimethyl sulfide (DMS) as another by-product (Fig. S13). Based on this information, we propose the following mechanism for the doping: As the DMSO-HBr adduct accepts electron(s) from the HOMO level of the organic molecule, the activated DMSO reduces to DMS, one of the by-products. The oxidation states of sulfur in DMSO and DMS are 0 and -2, respectively. The positive charge on the host organic cation is counterbalanced by the bromide anion from HBr. The oxygen from DMSO and H from the HBr molecule then form H₂O, as another by-product. We show the probable mechanism schematically in Fig. 2c. Apart from the Br⁻ counterion, which must be retained in the film to retain charge neutrality, we highlight that the doping process does not leave behind the byproducts or unreacted dopants in the organic semiconductor matrix, which we confirm by the FTIR and XPS measurements on doped Spiro-OMeTAD films (see Fig. S14 and S15).

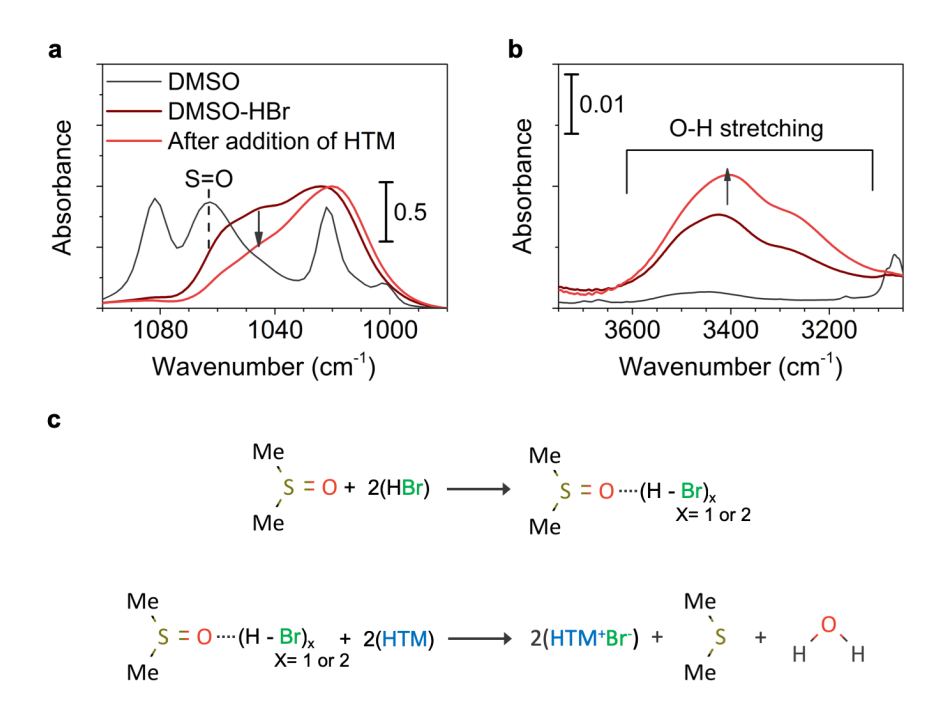


Figure 2| Mechanism of doping by DMSO-HBr adduct. a, b, FTIR spectrum of DMSO-HBr mixture in chlorobenzene, and after the addition of Spiro-OMeTAD showing the consumption of the adduct and formation of H_2O during the doping process. (a) the region of S=O absorbance (b) the region of the OH stretching absorbance. c, Proposed mechanism of the doping process.

In a similar fashion to DMSO-HBr, the DMSO-HCl adduct also induces p-type doping. However, we observe that the doping ability of the DMSO-HCl adduct is much weaker (Fig. S16). At the opposite end of the scale, the DMSO-HI adduct is unstable in ambient conditions and a considerable amount of I_2 is produced due to the oxidation of I^- in the solution, which we detect by UV-Vis spectroscopy (Fig. S17). We find that the DMSO-HX interaction strength progressively reduces with HI > HBr > HCl. This is a consequence of the reduction in the S-O bond length (Table S2) and increase in the S-O vibration frequency (Fig. S18) when going from I to CI, which we have ratified computationally.

Although the DMSO-HBr doping is clean and efficient, a critical factor for the utility of a doping process is that it must be stable under the conditions experienced during the manufacturing of additional layers in the device stack, and in typical end use of the devices, particularly at elevated temperatures. We use conductivity and ellipsometry-based optical measurements to investigate the thermal stability of the doped films. In order to assess if the counter ion diffuses between layers, we constructed devices with a double layer of doped and undoped HTMs, comprising a bottom-contact gold electrode on a Si substrate (Fig. 3a), a spin-coated doped layer of MeO-TPD, followed by a thermally evaporated layer of intrinsic MeO-TPD (See SI for the method).

If de-doping or migration of the doped organic molecule/counter ion occurs due to the thermal stress, we expect the conductivity and ellipsometric profiles of the films to change. As we show in Fig. 3b and Fig. S19a, we do not observe any change in the conductivity of the sample (doped with DMSO-HBr) not any change in the ellipsometric profile (phase difference Δ and amplitude ratio Ψ) over a period of 100 hours at 50 °C . We fit the ellipsometric profile of the thin-film used for thermal stability study as a bilayer stack with the bottom layer as doped MeO-TPD (~150 nm) and the top layer (~100 nm) as un-doped MeO-TPD. We fit both the layers for thicknesses first using Cauchy model and then for refractive indices using B-spline function. The Δ and Ψ spectra fit well to the expected double-layer stack of doped and intrinsic MeO-TPD layers, both before and after the thermal stressing. For completeness, using an effective medium approximation 35 , we simulate the ellipsometric profile which would be expected if the doped and non-doped layers mix to form a single homogeneous film. The simulated profiles for the mixed films, are different than the observed profiles (Fig. S19b), confirming that the migration of the doped material (or counterion) does not happen during the 50°C 100 hour stress test.

To further study the impact of doping on the morphology of the organic films, which is highly relevant for device applications, we perform atomic force microscopy (AFM) measurement of MeO-TPD films with different doping concentrations and following different

levels of thermal stressing. We observe no significant changes in the topography (Fig. 3d and Fig. S20), as quantified by the root mean squared (RMS) roughness of the films, for the doped films as compared to the undoped films, both before and after thermal stressing.

Despite being stable at 50°C, as we show in Fig. 3c, when we raise the stressing temperature to 85 °C, i.e. above the glass transition temperature of pure MeO-TPD, we observe a decrease in the conductivity in films doped with DMSO-HBr adduct, indicating dedoping, presumably owing to the diffusion of Br and subsequent escape from the matrix as Br₂. HBr plays a dual role in the doping process - as an activator and then as a provider of the anion. Our doping mechanism should allow us to introduce other anions, specifically chosen for improved thermal stability of the doped material or for other properties, which would therefore be decoupled from the dopant. To demonstrate that such "decoupling" of the dopant and counterion is feasible, we choose a combination of 10-camphorsulfonic acid (CSA), DMSO and HBr. We estimate via a Van der Waals surface calculation that the counter ion, camphorsulfonate, is ~8.5 times bulkier than bromide³⁶. The larger size of camphorsulfonate can likely reduce the diffusivity and volatility issues associated with bromide. We show the doping ability of the DMSO-HBr-CSA system in Spiro-OMeTAD and MeO-TPD by absorbance, conductivity, UPS and XPS studies (see Fig. S21-S24). No doping occur in Spiro-OMeTAD solution when we add DMSO-CSA only, unlike DMSO-HBr (see Fig. S25). However, we only need to add a small volume of aqueous HBr (i.e. ~9 mol% with respect to CSA) to "activate" the doping process. We determine that the doping efficiency of the DMSO-HBr-CSA system is ~22% (with respect to the added CSA molecules) for Spiro-OMeTAD from the optical absorbance change (see Fig. S21). For the films doped with DMSO-HBr-CSA, we observe no significant change in the conductivity (Fig. 3b and 3c) and morphology (Fig. 3d and Fig. S26) with prolonged thermal stressing, even at higher elevated temperatures of 100 °C. We present here only one example for the counterion exchange, but in principle, many other counterions tailored to specific needs could also be used.

We rationalize the doping process by the DMSO-HBr-CSA system considering that while DMSO and HBr form the adduct responsible for doping, CSA can provide the counter ion in the form of 10-camphorsulfonate and the HBr can be subsequently regenerated for further doping (Fig. S27). We note that our new doping process can also be used to produce very "clean" molecular organic semiconductor salts, such as Spiro-OMeTAD+TFSI-, which have been used as efficient and stable dopants in recent reports^{37,38}.

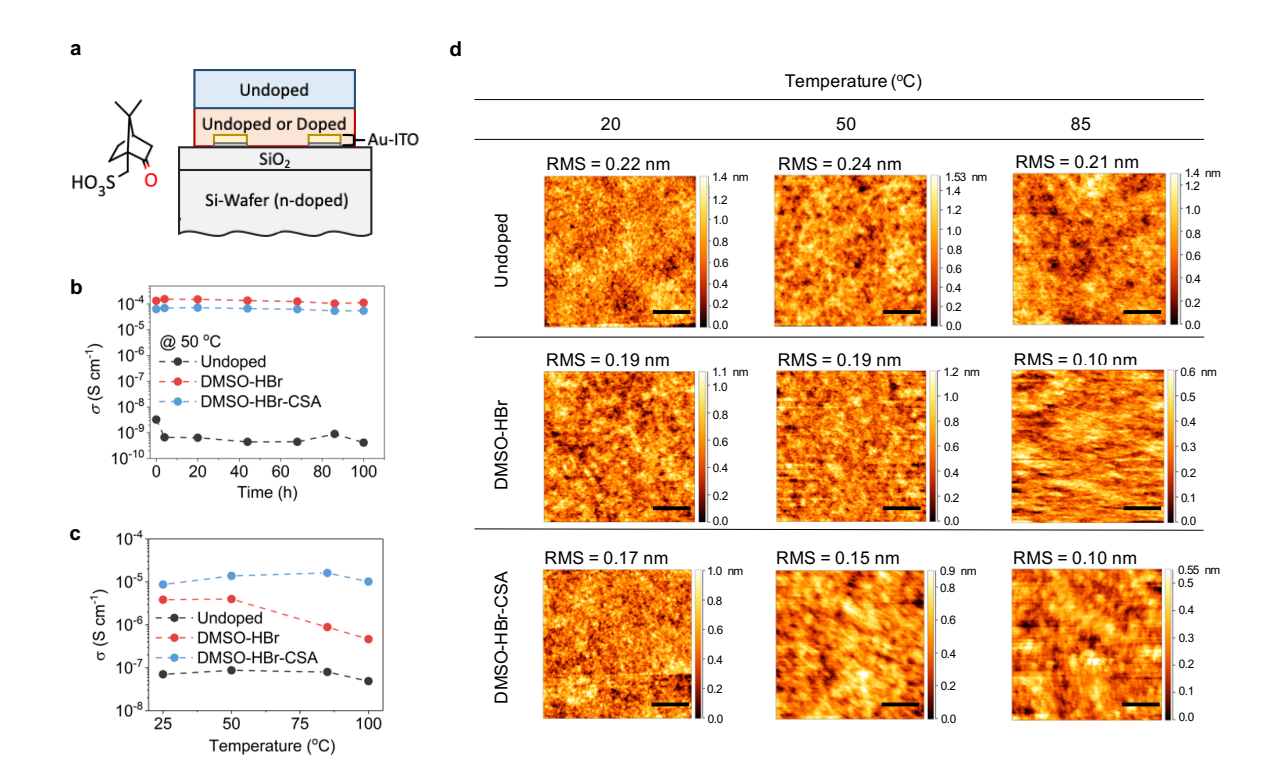


Figure 3| Thermal stability of the doped MeO-TPD films. a, Chemical structure of camphorsulfonic acid (CSA) and schematic illustration of geometry to evaluate thermal stability of dopants by the conductivity measurement. **b**, Conductivity of the MeO-TPD films doped with DMSO-HBr and DMSO-HBr-CSA after thermal stressing at 50 °C for 100 hours. **c**, Conductivity (at room temperature) of undoped MeO-TPD films and doped MeO-TPD film with DMSO-HBr and DMSO-HBr-CSA after stressing at different temperatures for 10 minutes on a hotplate in a nitrogen filled glove box. **d**, Atomic force microscope (AFM) topography images of the undoped and doped MeO-TPD films. The AFM images are taken after the films are incubated at 20, 50 and 85 °C for 10 minutes. The scale bar is 500 nm. Root Mean Square (RMS) height variation is evaluated over 2×2μm² in each AFM image.

One of the primary means to minimize contact resistance and create diode-like behaviour in semiconductor devices is to employ graded or a-symmetric doping, with distinct regions of high and low levels of p or n-type doping, with the highly doped region in contact with the electrode material^{20,39–42}. Analogously, a key breakthrough for OLEDs, pioneered by Leo and co-workers, has been the controlled p and n-type doping of organic charge transport materials, and combining this with the deposition of multiple layers of different organic semiconductors upon one another⁴³. For OLEDs, this is usually done via thermal evaporation of the organic semiconductors in vacuum, where layers of different compositions can be deposited upon each other^{44,45}. Employing double layers of doped and intrinsic p and n-type charge extraction layers, has also led to improved efficiency of vapour deposited perovskite solar cells⁴⁰.

For solution based processes, it is challenging to coat two subsequent layers on top of each other due to the common solubility of the host and dopants, without introducing more complicated chemistries such as molecular cross-linking to make the underlying film insoluble. Even with cross-linking of the host, the dopant must not diffuse into the adjacent layers, neither in manufacture nor in use. Here, we explore the possibility of asymmetric doping (i.e. the doping is predominantly at one interface) via our adduct methods. To that end, we prepare "hole-only" device with a stack of FTO/Poly-TPD (350 nm)/Au (See SI for the detail of sample preparation) where we introduce a CSA-DMSO-HBr layer (via solution process) either at the interface between Poly-TPD and Au or at the interface between Poly-TPD and FTO.

In Fig. 4a-c, we show the J-V curves of the hole-only devices where the interface and bulk are doped differently for each device. In Fig. 4a, the current density in the positive bias (i.e., hole injection from the Au electrode) clearly is higher for the device with doped Poly-TPD:Au interface when compared to the undoped device. For the doped device, the current density increases with the dopant concentration in the doped layer, which we control via the concentration of the CSA (see Fig. S28a). Under negative bias conditions (i.e., hole injection from the FTO side), the current densities are similar for both the asymmetrically doped and undoped devices. As would be expected for the case of interface doping, we observe the opposite trend in the *J-V* curves (Fig. 4 (b) and Fig. S28b) for the devices where the doping is introduced at the FTO: Poly-TPD interface, where we observe increased current density for the interface-doped device under negative bias conditions. As we show in Fig. 4c,

for homogeneous doping, the increase in the current densities are similar for both negative and positive bias conditions.

To explore the localization of the space charge regions in the hole-only devices with interface doping, we perform capacitance-voltage measurements (see Fig. S29) and use Mott-Schottky analysis to estimate the acceptor density (N_A) as a function of the depletion width (w) from the conductive electrode-organic semiconductor junction (See SI for the details and description of the Mott-Schottky analysis)^{46–48}. When profiling the acceptor density in the proximity of the doped interfaces, we find that the N_A values in the devices for the doped Poly-TPD:Au interface (Fig. 4d) and doped FTO:Poly-TPD interface (Fig. 4e) exhibit a gradient profile. The N_A follows a gradual decrease away from these doped interfaces, followed by a steep increase when the calculated depletion width approaches the width of the complete diode. In Fig. 4f, we show the N_A profile of the homogeneously doped devices. Compared to the undoped device (Fig. S30), we see a higher N_A value for the homogeneously doped device. Since the calculated N_A increased strongly for all devices (doped or undoped) when the depletion width approaches the total film thickness, (whether this is approaching the Au or FTO electrode) we assume that this is an artefact of the measurement, rather than carrying real physical meaning.

Our capacitance-voltage results are consistent with asymmetric doping, but are subject to a model and the assumption of which contact is the primary contact being probed. To further investigate the asymmetric doping, we perform Secondary Ion Mass Spectrometry (SIMS) measurements of the doped and undoped films. Here we use silicon as a substrate. Since the HTM (MeO-TPD) does not contain sulphur, mapping of sulphur signal can be used to determine the distribution of the counter ions (CSA-) in the doped film. In Fig. S31-32 we show the depth profiles of sulphur in undoped as well as doped films. For the films which we intended to dope at the top surface, we observe a significant enhancement of the sulphur signal at this interface (Fig. S31b), and for the films doped at the buried HTM:Si interface, we observe sulphur enrichment at this buried interface (Fig. S32). This enhancement of sulphur at the intended interfaces further confirms asymmetric doping. We do note that there is a relatively small increase in the sulphur signal at the opposite interfaces to where the doping was intended, which indicates some degree of diffusion of the counter-ions during fabrication.

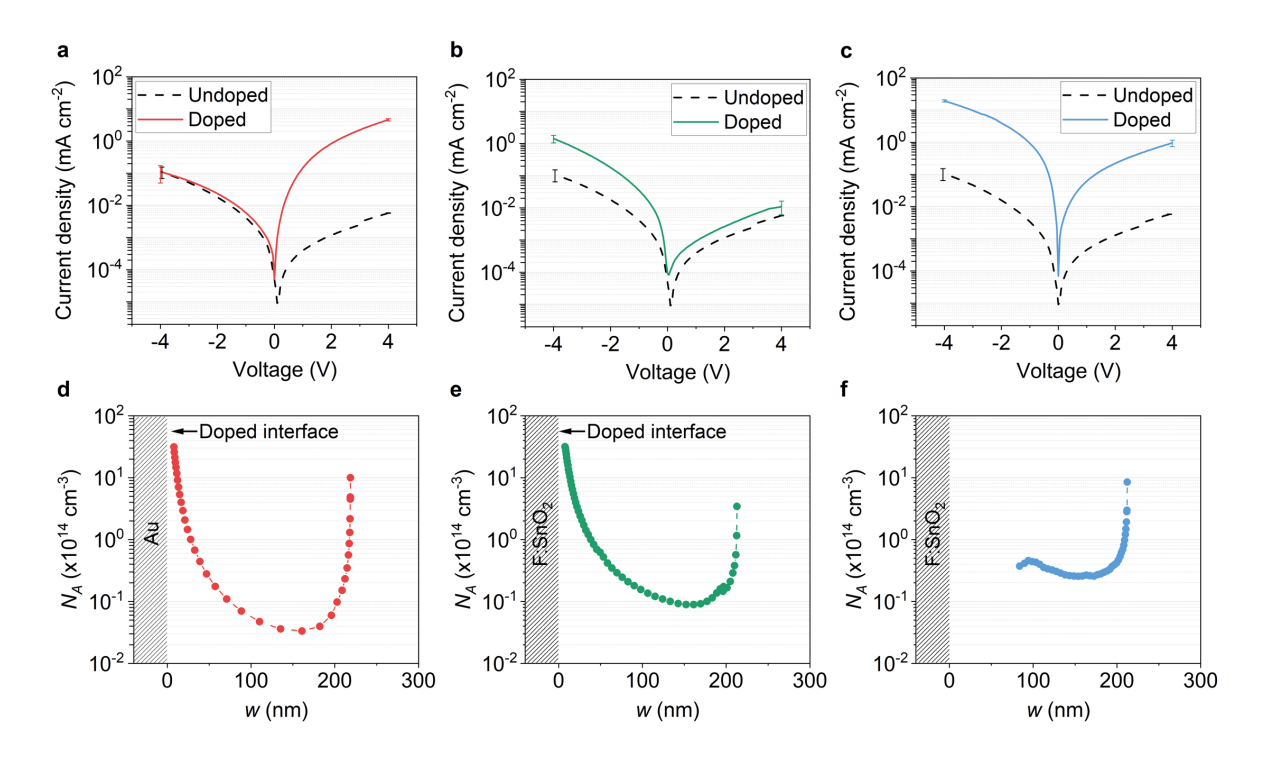


Figure 4| Asymmetric doping in hole-only devices. a, **b**, **c**, Current density-voltage curves of the hole-only devices (**a**) doping at Poly-TPD: Au interface (**b**) at FTO: Poly-TPD interface, and (**c**) homogeneous doping. **d**, **e**, **f** Acceptor density (N_A) as a function of depletion width (w) in hole-only devices, (**d**) doped at the Poly-TPD:Au interface, (**e**) doped at the FTO:Poly-TPD interface, (**f**) homogeneously doped.

We now demonstrate the utility of the doping methods in three types of optoelectronic devices which benefit from doped charge transport layers: organic thin film transistor (OTFT), perovskite solar cells and OLEDs (see Fig. 5a for the device architectures).

It is known that semiconductor doping plays a critical role for enhancing many performance facets of an OTFT, such as facilitating charge transport, reducing contact resistance, and improving operational stability^{49–51}. We fabricate indacenodithiophene-benzothiadiazole (C_{16} IDT-BT) based organic thin-film transistors (OTFTs) in a top-gate bottom-contact (TG-BC) device architecture (Fig. 5a)⁵². Fig. 5b shows the transfer current-voltage characteristics measured from OTFTs fabricated using pristine and moderately- and heavily-doped C_{16} IDT-BT based on the solution-processed DMSO-HBr adduct doping approach (denoted as DMSO-HBr (M) and DMSO-HBr (H), respectively). We observe significant changes of several electrical characteristics, including higher current levels and positively shifted turn-on voltages (V_{ON}) due to p-doping. In Supplementary Table S3 and in

Fig. S33, we summarise the performance parameters from the transfer characteristics and provide the detailed analysis on the areal trap density (ΔN_{tr} , as compared to the undoped device) to and the trap concentration per unit energy (D_{tr}). We achieve a clear improvement in field-effect mobility (Supplementary Table S3) by the adduct-based doping. We further confirm that the DMSO-HBr-CSA adduct doping assist hole transport in OTFTs in Fig. S34 and Table S4.

For perovskite solar cells, we use Spiro-OMeTAD as the HTM with the presented doping methods here and compare to other doping methods commonly used such as doping with Li-TFSI-oxygen or Co(III)TFSI (see Fig. S35 ad Table S5). Note that all high-performance perovskite solar cells contain Li-TFSI and 4-tert-butylpyridine (*t*BP). In Fig. 5c, we show the *J-V* curves and steady-state power output (SPO) of our best-performing solar cells, where the HTM is doped with the DMSO-adduct based dopant or Li-TFSI-oxygen, measured under simulated sunlight. We find that the devices where the HTM is doped with DMSO-HBr (a combined solution and vapor process method) or DMSO-HBr-CSA (solution process) show significantly improved power conversion efficiency (PCE) and SPO as compared to the commonly used Li-TFSI-oxygen doping or cobalt-complex doping (see Fig. 5c). We summarize the PV performance parameters in Table 1. In the SI, we show additional information to corroborate the PV properties with our new doping, such as cross-sectional scanning electron micrograph of devices, external quantum efficiency (EQE), and forward and revere scan directions of the JV curves (see Fig. S36 - S38 and Table S6).

To further illustrate the compatibility with other HTMs, we also demonstrate the doping capability of DMSO-HBr-CSA on Poly[bis(4-phenyl)(2,4,6-trimethylphenyl)amine (PTAA) in n-i-p perovskite solar cells, without tBP and Li-TFSI (Fig. S39). The device containing the DMSO-HBr-CSA doped PTAA exhibits an improvement of current density, fill factor and ensuing efficiency, as compared to an un-doped PTAA layer.

As we have shown in Fig. 1e, the Fermi level in the HTM monotonically shifts closer to the HOMO level onset with increasing dopant concentration. In the complete solar cell, the Fermi level alignment between the HTM and the quasi-Fermi level for holes in the perovskite absorber layer, and between the HTM and the Fermi level of the metallic electrode, are likely to improve with increased doping density. Therefore, the increased V_{oc} of the solar cells suggests an improved energetic alignment across these interfaces due to doping. We can also consider that the improved doping of the HTM has improved the "selectivity" for hole extraction, which is expected to result in an increase in open-circuit voltage.⁵³ On the other hand, the improvement in fill factor, is consistent with reduced series resistance in the cell, resulting from increased conductivity of the HTM. Therefore, both these effects, Fermi level

deepening, and increased conductivity, appear to be contributing to the improved performance in the solar cells.

We have provided above justifications as to why the FF and open-circuit voltage improve with our adduct-based doping strategy. However, the increase in J_{SC} is less intuitive. There are many examples in the literature of perovskite solar cells, where increased J_{SC} is observed with increased doping of the HTM^{30,54–56}. This is most clearly illustrated by showing the JV curves for a perovskite solar cell with spiro-OMeTAD and no doping of the HTM, as we show in Fig. S40. In this instance, the J_{SC} is approximately half the value of J_{SC} in the device with the doped HTM. However, upon applying a 2.5V reverse bias, the photocurrents of the doped and non-doped devices coincide. If this short-circuit current density was solely limited by series resistance, we would expect the JV curve to be a straight line from open-circuit to short-circuit. However, there remains some curvature in the JV curve of the un-doped device, indicating that this is not simply a series resistance limitation. This therefore illustrates that doping of the HTM does influence charge extraction under all working conditions, including short-circuit. Without doping, an external applied electric field appears to be required in order to extract all photogenerated carriers. This indicates a charge extraction barrier being present with the undoped HTM.

To illustrate functionality of other optoelectronic devices, we fabricated OLEDs with the prototypical Tris-(8-hydroxyquinoline)aluminum (Alq₃) as the emitting material, sandwiched between MeO-TPD as the hole transport layer and bathophenanthroline (BPhen) as the electron transport layer (see Fig 5 a). We show the luminance-voltage curves in Fig. 5 d and the J-V curves in the inset. We observe an increase in current density for any given applied voltage in forward bias, for OLEDs where the MeO-TPD layer is doped with DMSO-HBr or DMSO-HBr-CSA, in comparison to the undoped device. At ~18 V applied voltage, electroluminescence (EL) present at 552 nm for all of the devices (see Fig. S41) and both doped devices display increased luminance as compared to the undoped device. We attribute the improvement in the intensity of EL to the improved charge injection with the doped HTMs. We also evaluate the performance of the OLED doped with F4TCNQ as a typical p-dopant (Fig. S42). We find that the OLEDs prepared with the widely used p-dopant F4TCNQ perform comparably to our DMSO adduct-based dopant. Even though the OLEDs doped with DMSO adduct-based dopant are not completely optimized, it is clear that the presented doping method and materials could be useful in OLEDs as well in perovskite solar cells, while also retaining distinct advantages.

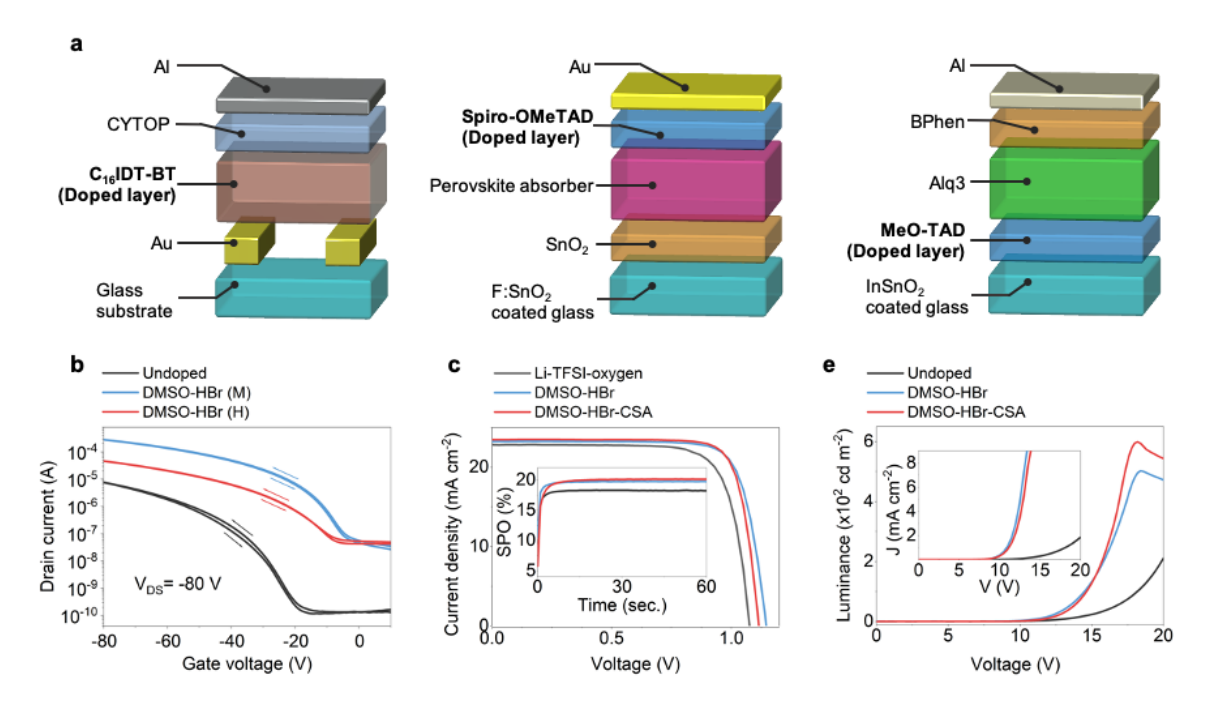


Figure 5| Usage of adduct-based dopants in optoelectronic devices. a, Schematic of the organic thin film transistor (OTFT: left), perovskite photovoltaic device (Middle) and the organic light emitting device (OLED: right).**b**, Current-voltage characteristics of DMSO-HBr-doped C16 IDT-BT based OTFT **c**, Current density-voltage curves of the solar cells with different dopants and counterions, Inset: stabilized power output (SPO) for the respective perovskite solar cells at a fixed maximum power point voltage. **d**, luminescence-voltage curve for the OLEDs with different dopants and counterions, inset: Current density-voltage curves of the OLEDs.

Table 1| Device performance parameters of perovskite solar cells doped with DMSO-adducts based dopant and Li-TFSI-Oxygen.

Doping method	Jsc (mA cm ⁻²)	Voc (V)	FF	PCE (%)	Rs (Ohm.)	SPO (%)
Li-TFSI-oxygen	22.8	1.08	0.76	18.7	39.9	18.2
DMSO-HBr DMSO-HBr-CSA	23.2 23.5	1.14 1.11	0.79 0.81	21.1 21.3	38.9 32.5	19.8 20.1

In conclusion, we have demonstrated a DMSO-adduct based p-doping scheme, applicable to a variety of organic HTMs ranging from small molecules to polymers. From understanding the doping mechanism, we have decoupled the dopant from the counter ions, allowing the electronic and physical properties and thermal stability of the doped HTM to be tuned separately. We also demonstrate that asymmetric doping is possible, using our adduct based doping method. Finally, we have shown the usage of the doped organic layers organic thin film transistors, perovskite solar cells and in OLED showing improvements in performance in all the cases. The p-doping method which we have presented here is not restricted to the DMSO-HBr adduct. In principle, it can be extended to other adduct systems where different sulfoxide containing molecules in combination with different activators should be feasible, highlighting a new avenue to pursue for controlled doping of organic semiconductors.

Acknowledgements:

This research has mainly received funding from the European Commission (PERTPV-agreement number 763977) and EPSRC (EP/M005143/1).

M.R. has received funding from the EC FP 7 MSCA - Career Integration Grant (630864) and EPSRC (EP/M015173/1). R.W. is supported by EPSRC CDT Plastic Electronics (EP/L016702/1). P.N. acknowledges the support via intramural funding at TIFR-Hyderabad and from SERB India core research grant (CRG/2020/003877).

F.Z., X.L. and A.K. acknowledge funding from National Science Foundation under grants DMR-1506097 and DMR-1807797. S.N. acknowledgs Marie Skłodowska-Curie actions individual fellowships (grant agreement number 659306). T.M. and V.G. acknowledge funding from European Regional Development Fund (project No 01.2.2-LMT-K-718-03-0040) under grant agreement with the Research Council of Lithuania (LMTLT). We thank I. McPherson for his help in mass spectrometry measurement

Contributions: NS and PN conceived and executed the initial proof of concept experiments and unravel the mechanism of doping. PN proposed dopant system. HJS proposed the graded doping and NS designed and performed the experiments. NS and RW performed the conductivity measurements. NS, RW performed the doping stability test under the supervision of MR. SK performed the ellipsometry measurements, analyses and simulation under the supervision of MR. RW fabricated OLEDs under supervision of MR and NS fabricated all other the devices used in this work. SN and PN performed the ATR-FTIR measurements. FZ and XL did the UPS, XPS and Kelvin probe measurements under the supervision of AK. FZ did the AFM measurements. JL did the Nano-SIMS measurements with inputs from PN and NS. C G planned and helped interpreting the Nano-SIMS measurements. NS and Y-HL performed

the capacitance-voltage measurements. HB performed the quantum chemical calculations. TM conducted synthesis of the HTM V886, VG supervised the synthesis. NS and PN wrote the first draft. All the authors contributed to the analysis of the results and discussion of the content and revisions of the manuscript. PN and HJS supervised the project. AB fabricated OTFTs and performed electrical characterisation under the supervision of TDA. TDA, Y-HL and AB interpreted the results and provided the analysis of OTFTs.

Competing interest: A patent based on this work has been filed (International application number: PCT/GB2018/053014) by the University of Oxford.

References:

- 1. Granström, M. *et al.* Laminated fabrication of polymeric photovoltaic diodes. *Nature* **395**, 257 (1998).
- 2. Halls, J. J. M. *et al.* Efficient photodiodes from interpenetrating polymer networks. *Nature* **376**, 498 (1995).
- 3. Sirringhaus, H. *et al.* Two-dimensional charge transport in self-organized, high-mobility conjugated polymers. *Nature* **401**, 685 (1999).
- 4. Tang, C. W. & Vanslyke, S. A. Organic electroluminescent diodes. *Appl. Phys. Lett.* **51**, 913–915 (1987).
- 5. Yu, G., Gao, J., Hummelen, J. C., Wudl, F. & Heeger, A. J. Polymer Photovoltaic Cells: Enhanced Efficiencies via a Network of Internal Donor-Acceptor Heterojunctions. *Science (80-.).* **270**, 1789 LP 1791 (1995).
- 6. Blochwitz, J., Pfeiffer, M., Fritz, T. & Leo, K. Low voltage organic light emitting diodes featuring doped phthalocyanine as hole transport material. *Appl. Phys. Lett.* **73**, 729–731 (1998).
- 7. Maennig, B. *et al.* Controlled p -type doping of polycrystalline and amorphous organic layers: Self-consistent description of conductivity and field-effect mobility by a microscopic percolation model. **64**, 1–9 (2001).
- 8. Godet, C. Variable range hopping revisited: the case of an exponential distribution of localized states. *J. Non. Cryst. Solids* **302**, 333–338 (2002).
- 9. Rubel, O., Baranovskii, S. D., Thomas, P. & Yamasaki, S. Concentration dependence of the hopping mobility in disor- dered organic solids. *phys. stat. sol.* **171**, 168–171 (2004).
- 10. Blochwitz, J. *et al.* Interface electronic structure of organic semiconductors with controlled doping levels. *Org. Electron.* **2**, 97–104 (2001).

- 11. Gao, W. & Kahn, A. Controlled p-doping of zinc phthalocyanine by coevaporation with tetrafluorotetracyanoquinodimethane: A direct and inverse photoemission study. *Appl. Phys. Lett.* **79**, 4040–4042 (2001).
- 12. Harada, K. *et al.* Organic Homojunction Diodes with a High Built-in Potential: Interpretation of the Current-Voltage Characteristics by a Generalized Einstein Relation. *Phys. Rev. Lett.* **94**, 36601 (2005).
- 13. Chan, C. K., Zhao, W., Barlow, S., Marder, S. & Kahn, A. Decamethylcobaltocene as an efficient n-dopant in organic electronic materials and devices. *Org. Electron.* **9**, 575–581 (2008).
- 14. Lin, X. *et al.* Beating the thermodynamic limit with photo-activation of n-doping in organic semiconductors. *Nat. Mater.* **16**, 1209 (2017).
- 15. Tietze, M. L. *et al.* Elementary steps in electrical doping of organic semiconductors. *Nat. Commun.* **9**, 1182 (2018).
- 16. Tietze, M. L., Burtone, L., Riede, M., Lüssem, B. & Leo, K. Fermi level shift and doping efficiency in p -doped small molecule organic semiconductors: A photoelectron spectroscopy and theoretical study. *Phys. Rev. B* **035320**, 1–12 (2012).
- 17. Li, J. et al. Measurement of Small Molecular Dopant F4TCNQ and C60F36 Diffusion in Organic Bilayer Architectures. ACS Appl. Mater. Interfaces 7, 28420–28428 (2015).
- 18. Møndez, H. *et al.* Doping of Organic Semiconductors: Impact of Dopant Strength and Electronic Coupling. *Angew. Chemie Int. Ed.* **52**, 7751–7755 (2013).
- 19. Jacobs, I. E. & Moulé, A. J. Controlling Molecular Doping in Organic Semiconductors. *Adv. Mater.* **29**, 1–39 (2017).
- 20. Kolesov, V. A. *et al.* Solution-based electrical doping of semiconducting polymer films over a limited depth. *Nat. Mater.* **16**, 474–481 (2017).
- 21. Yusubov, M. S., Filimonov, V. D. & Ogorodnikov, V. D. Dimethyl sulfoxide-hydrobromic acid as a novel reagent for convenient oxidation on a preparative scale of stilbenes and some derivatives of diphenylethane to benzils. *Bull. Acad. Sci. USSR, Div. Chem. Sci.* **40**, 766–770 (1991).
- 22. Lee, T. V. Oxidation Adjacent to Oxygen of Alcohols by Activated DMSO Methods. *Compr. Org. Synth.* 291–303 (1991). doi:10.1016/B978-0-08-052349-1.00191-8
- 23. Floyd, M. B., Du, M. T., Fabio, P. F., Jacob, L. A. & Johnson, B. D. The oxidation of acetophenones to arylglyoxals with aqueous hydrobromic acid in dimethyl sulfoxide. *J. Org. Chem.* **50**, 5022–5027 (1985).
- 24. Sakai, N. *et al.* Solution-Processed Cesium Hexabromopalladate(IV), Cs2PdBr6, for Optoelectronic Applications. *J. Am. Chem. Soc.* **139**, 6030–6033 (2017).

- 25. Cappel, U. B., Daeneke, T. & Bach, U. Oxygen-Induced Doping of Spiro-MeOTAD in Solid-State Dye-Sensitized Solar Cells and Its Impact on Device Performance. *Nano Lett.* **12**, 4925–4931 (2012).
- 26. Burschka, J. *et al.* Tris(2-(1H-pyrazol-1-yl)pyridine)cobalt(III) as p-Type Dopant for Organic Semiconductors and Its Application in Highly Efficient Solid-State Dye-Sensitized Solar Cells. *J. Am. Chem. Soc.* **133**, 18042–18045 (2011).
- 27. Planells, M. *et al.* Diacetylene bridged triphenylamines as hole transport materials for solid state dye sensitized solar cells. *J. Mater. Chem. A* **1**, 6949–6960 (2013).
- 28. Abate, A. *et al.* Protic Ionic Liquids as p-Dopant for Organic Hole Transporting Materials and Their Application in High Efficiency Hybrid Solar Cells. *J. Am. Chem. Soc.* **135**, 13538–13548 (2013).
- 29. Pellaroque, A. *et al.* Efficient and Stable Perovskite Solar Cells Using Molybdenum Tris(dithiolene)s as p-Dopants for Spiro-OMeTAD. *ACS Energy Lett.* **2**, 2044–2050 (2017).
- 30. Nguyen, W. H., Bailie, C. D., Unger, E. L. & McGehee, M. D. Enhancing the Hole-Conductivity of Spiro-OMeTAD without Oxygen or Lithium Salts by Using Spiro(TFSI)2 in Perovskite and Dye-Sensitized Solar Cells. *J. Am. Chem. Soc.* **136**, 10996–11001 (2014).
- 31. Chen, C. et al. Cu(II) Complexes as p-Type Dopants in Efficient Perovskite Solar Cells. ACS Energy Lett. **2**, 497–503 (2017).
- 32. Ono, L. K. *et al.* Air-Exposure-Induced Gas-Molecule Incorporation into Spiro-MeOTAD Films. *J. Phys. Chem. Lett.* **5**, 1374–1379 (2014).
- 33. Fawcett, W. R. & Kloss, A. A. Solvent-Induced Frequency Shifts in the Infrared Spectrum of Dimethyl Sulfoxide in Organic Solvents. *J. Phys. Chem.* **100**, 2019–2024 (1996).
- 34. Wallace, V. M., Dhumal, N. R., Zehentbauer, F. M., Kim, H. J. & Kiefer, J. Revisiting the Aqueous Solutions of Dimethyl Sulfoxide by Spectroscopy in the Mid- and Near-Infrared: Experiments and Car–Parrinello Simulations. *J. Phys. Chem. B* **119**, 14780–14789 (2015).
- 35. Fujiwara, H. Spectroscopic Ellipsometry: Principles and Applications. *John Wiley & Sons, Ltd* (2007). doi:doi:10.1002/9780470060193.fmatter
- 36. Zhao, Y. H., Abraham, M. H. & Zissimos, A. M. Fast Calculation of van der Waals Volume as a Sum of Atomic and Bond Contributions and Its Application to Drug Compounds. *J. Org. Chem.* **68**, 7368–7373 (2003).

- 37. Christians, J. A. *et al.* Tailored interfaces of unencapsulated perovskite solar cells for >1,000 hour operational stability. *Nat. Energy* **3**, 68–74 (2018).
- 38. Leijtens, T. *et al.* Hydrophobic Organic Hole Transporters for Improved Moisture Resistance in Metal Halide Perovskite Solar Cells. *ACS Appl. Mater. Interfaces* **8**, 5981–5989 (2016).
- 39. Kang, K. *et al.* 2D coherent charge transport in highly ordered conducting polymers doped by solid state diffusion. *Nat. Mater.* **15**, 896 (2016).
- 40. Ávila, J. *et al.* High voltage vacuum-deposited CH3NH3PbI3–CH3NH3PbI3 tandem solar cells. *Energy Environ. Sci.* **11**, 3292–3297 (2018).
- 41. Abdi-Jalebi, M. *et al.* Charge extraction via graded doping of hole transport layers gives highly luminescent and stable metal halide perovskite devices. *Sci. Adv.* **5**, eaav2012 (2019).
- 42. Wanlass, M. Systems and methods for advanced ultra-high-performance InP solar cells. (2017).
- 43. Walzer, K., Maennig, B., Pfeiffer, M. & Leo, K. Highly Efficient Organic Devices Based on Electrically Doped Transport Layers. *Chem. Rev.* **107**, 1233–1271 (2007).
- 44. Pfeiffer, M., Beyer, A., Fritz, T. & Leo, K. Controlled doping of phthalocyanine layers by cosublimation with acceptor molecules: A systematic Seebeck and conductivity study. *Appl. Phys. Lett.* **73**, 3202–3204 (1998).
- 45. Nollau, A., Pfeiffer, M., Fritz, T. & Leo, K. Controlled n-type doping of a molecular organic semiconductor: Naphthalenetetracarboxylic dianhydride (NTCDA) doped with bis(ethylenedithio)-tetrathiafulvalene (BEDT-TTF). *J. Appl. Phys.* **87**, 4340–4343 (2000).
- 46. Kirchartz, T. *et al.* Sensitivity of the Mott Schottky Analysis in Organic Solar Cells. *J. Phys. Chem. C* **116**, 7672–7680 (2012).
- 47. Deledalle, F. *et al.* Understanding the Effect of Unintentional Doping on Transport Optimization and Analysis in Efficient Organic Bulk-Heterojunction Solar Cells. *Phys. Rev. X* **5**, 11032 (2015).
- 48. Zonno, I., Martinez-Otero, A., Hebig, J. & Kirchartz, T. Understanding Mott-Schottky Measurements under Illumination in Organic Bulk Heterojunction Solar Cells. *Phys. Rev. Appl.* **7**, 034018 (2017).
- 49. Paterson, A. F. *et al.* The Impact of Molecular p-Doping on Charge Transport in High-Mobility Small-Molecule/Polymer Blend Organic Transistors. *Adv. Electron. Mater.* **4**, 1700464 (2018).

- 50. Panidi, J. *et al.* Remarkable Enhancement of the Hole Mobility in Several Organic Small-Molecules, Polymers, and Small-Molecule:Polymer Blend Transistors by Simple Admixing of the Lewis Acid p-Dopant B(C6F5)3. *Adv. Sci.* **5**, 1700290 (2018).
- 51. Paterson, A. F. *et al.* Addition of the Lewis Acid Zn(C6F5)2 Enables Organic Transistors with a Maximum Hole Mobility in Excess of 20 cm2 V–1 s–1. *Adv. Mater.* **31**, 1900871 (2019).
- 52. Lin, Y.-H. *et al.* Deciphering photocarrier dynamics for tuneable high-performance perovskite-organic semiconductor heterojunction phototransistors. *Nat. Commun.* **10**, 4475 (2019).
- 53. Onno, A., Chen, C., Koswatta, P., Boccard, M. & Holman, Z. C. Passivation, conductivity, and selectivity in solar cell contacts: Concepts and simulations based on a unified partial-resistances framework. *J. Appl. Phys.* **126**, 183103 (2019).
- 54. Xi, H. *et al.* Performance Enhancement of Planar Heterojunction Perovskite Solar Cells through Tuning the Doping Properties of Hole-Transporting Materials. *ACS Omega* **2**, 326–336 (2017).
- 55. Wong-Stringer, M. *et al.* Efficient perovskite photovoltaic devices using chemically doped PCDTBT as a hole-transport material. *J. Mater. Chem. A* **5**, 15714–15723 (2017).
- 56. Ulfa, M., Pauporté, T., Bui, T.-T. & Goubard, F. Impact of Organic Hole Transporting Material and Doping on the Electrical Response of Perovskite Solar Cells. *J. Phys. Chem. C* **122**, 11651–11658 (2018).